ACS APPLIED MATERIALS & INTERFACES

RESEARCH ARTICLE

www.acsami.org

Nanoporous Polyethylene Thin Films Templated by Polymeric Bicontinuous Microemulsions: Evolution of Morphology on Non-neutral Substrates

Brad H. Jones,[†] Kai-Yuan Cheng,[†] Russell J. Holmes,[†] and Timothy P. Lodge*[,†,‡]

[†]Department of Chemical Engineering and Materials Science and [‡]Department of Chemistry, University of Minnesota, Minneapolis, Minnesota 55455, United States

ABSTRACT: Polymeric bicontinuous microemulsions (BμE), found in well-designed ternary blends of two homopolymers and a diblock copolymer, have been extensively studied in the bulk, for example, as versatile templates for the synthesis of nanoporous materials. However, there have been few reports regarding BμE-forming blends as films and the potential impact of confinement on the morphology of such blends. We have investigated the morphology of ternary blends of polyethylene (PE), poly(ethylene-*alt*-propylene) (PEP), and poly(ethylene-*b*-ethylene-*alt*-propylene) (PE−PEP) on a variety of substrates. The films were rendered nanoporous by selective extraction of the PEP component, which also created contrast for scanning electron microscopy (SEM). Blends that form BμEs in the bulk were found to undergo an evolution of morphology from a BμE to a macro-phase separated state, induced by the segregation of blend components to the film interfaces. The dynamics of the transformation are accelerated by decreasing film thickness. The results presented indicate that BμEs can be kinetically trapped on arbitrary substrates, which has important implications for the production of bicontinuous, nanoporous films.

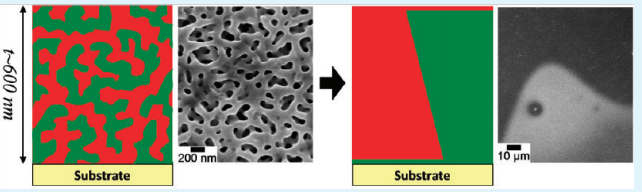

KEYWORDS: nanoporous polyethylene, bicontinuous microemulsion, ternary polymer blend, thin film morphology, indium tin oxide, scanning electron microscopy

INTRODUCTION

Materials consisting of two or more phases assembled in periodic, nanoscale structures represent a substantial area of current research. In particular, bicontinuous structures are distinctive, biphasic arrangements where each phase is independently continuous in three dimensions.[1] If one of the phases comprises voids, the resultant material will contain a three-dimensionally interconnected network of pores with inherently high surface area. Such materials are of tremendous importance in many applications, including catalysis,[2] separations and drug delivery,[3] electronic devices,[4] and gas storage.[5] Therefore, there is a strong motivation to develop new or improved strategies for the synthesis of bicontinuous, nanoporous materials with well-defined pore shapes and sizes. In this respect, block polymers provide a relatively straightforward route. Various multiply continuous morphologies spontaneously form in appropriately designed block polymer or block polymer-containing liquids, which, due to the relatively slow dynamics inherent to macromolecules, can be readily trapped in a solid form by vitrification, crystallization, or other means.[6] The subsequent, selective removal of a specific block or component by chemical or thermal processes yields a nanoporous material, generally possessing a narrowly distributed pore size that is correlated with the molecular dimensions of the removed phase.[7,8]

A unique, bicontinuous morphology was discovered in 1997 in ternary blends of the homopolymers PE and PEP and their corresponding diblock copolymer PE−PEP.[9] This equilibrium morphology − a BμE − consisted of disordered networks of PE and PEP with local periodicity on the order of 100 nm. Subsequent work demonstrated that BμEs are universally found in ternary blends of type A/B/A−B, provided that the block copolymer is volumetrically symmetric, the homopolymers are of equal size and are mixed in equal volumes, and the block copolymer is larger than the homopolymers.[10−15] Under these constraints, the phase space of a blend can be described by temperature and the volume fraction of homopolymers, Φ_H, where $\Phi_H = \Phi_A + \Phi_B = 1 - \Phi_{A-B}$, as shown in Figure 1a. At high block copolymer content, the blend exhibits an order−disorder transition between microphase separated lamellae and a single-phase melt. As homopolymers are progressively added to the blend, the lamellae are swollen until their spacing diverges, at which point a BμE is stabilized by composition fluctuations.[16−18] The BμE exists over only a narrow channel of composition; with further addition of homopolymers, the block copolymer is unable to sufficiently stabilize the extensive interface of the BμE and the blend exhibits macroscopic phase separation.

We have recently demonstrated that BμEs are effective precursors for nanoporous materials. In one example, a polystyrene (PS)/polyisoprene (PI)/PS-PI BμE was captured by vitrification of the PS and rendered porous through a two-step sequence

Received: July 26, 2011
Accepted: September 1, 2011
Published: September 15, 2011

dx.doi.org/10.1021/am2009794 | *ACS Appl. Mater. Interfaces* 2011, 3, 4101–4111

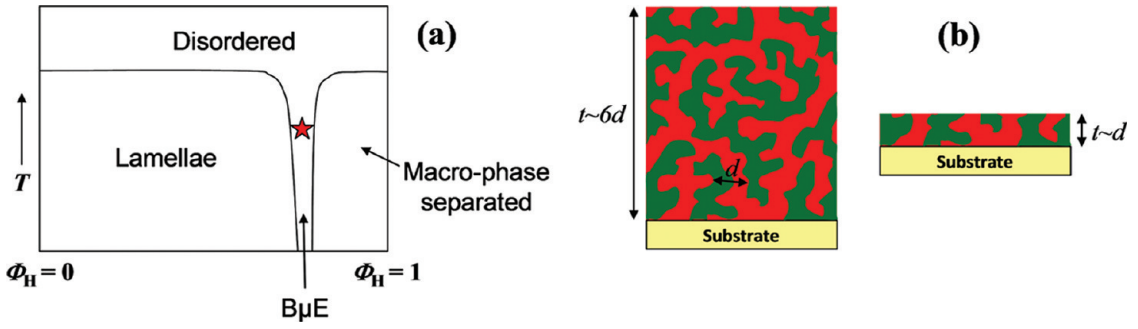

Figure 1. (a) Bulk phase diagram for symmetric, ternary A/B/A−B polymer blends. Φ_H is the volume fraction of homopolymers, $\Phi_H = \Phi_A + \Phi_B = 1 - \Phi_{A-B}$. The diblock copolymer is symmetric, the homopolymers are of equal size and are present in equal amounts, i.e., $\Phi_A = \Phi_B$. The diagram shown is for a copolymer to homopolymer size ratio of ~5.25; the same diagram applies for any ratio greater than unity, with the phase transitions shifted accordingly. A small region of coexistence separating the boundary between lamellae and disordered/BμE is not shown. The red star represents the blend composition and annealing temperature applied to the films studied in this work. (b) Cartoon depiction of the bulk BμE structure confined within films of two different thicknesses. The red and green colors indicate domains of A and B, respectively. The BμE is characterized by a domain spacing d of order 100 nm. The thicknesses t correspond to six domain spacings (left) and a single domain spacing (right). A and B appear as networks and isolated domains in the thicker and thinner films, respectively.

involving cross-linking of the PI and dissolution of the PS.[19] In another example, a PE/PEP/PE−PEP BμE was captured by crystallization of the PE and rendered porous simply by dissolution of the PEP.[20] The resultant nanoporous PE was used as a template in the synthesis of a variety of other nanoporous materials, including ceramics[21] and polymeric thermosets,[20] where the original BμE structure is replicated in the final product. These materials show well-defined and relatively narrowly distributed pore sizes of approximately 100 nm, making them particularly distinctive, since few techniques exist for the creation of uniformly shaped pores in this size range. To date, we have only reported the synthesis of monolithic materials; the extension of this BμE templating strategy to films could potentially enable new porous materials with applications including solar cells,[22−25] lithography,[26] low-dielectric constant materials,[27−29] separation membranes,[30−32] and antireflective coatings.[33−39]

Little is known about the phase behavior of such ternary blends when deposited as thin films on substrates. Specifically, the thickness of a film, t, may approach the bulk periodicity of a BμE, denoted by the domain spacing d,[40] where $d/2$ is the average size of an A or B domain. In this situation, it is unclear a priori as to whether the blend will adopt a bicontinuous morphology or will be driven to a different state of thermodynamic equilibrium. A cartoon depiction is shown of the bulk structure of a BμE confined within films of different thicknesses in Figure 1b. When t is significantly greater than d, the bicontinuous structure is clearly evident. When t is comparable to d, the connectivity in three dimensions is no longer obvious from this simple, two-dimensional representation. Previous simulations and experiments have demonstrated that the bicontinuous double gyroid morphology, found in asymmetric diblock copolymers, is preempted by morphologies with two-dimensional periodicity when confined in at least one dimension.[41,42] However, BμEs differ from the latter in their degree of ordering and the thermodynamic basis for their formation, so the effect of confinement may be significantly different. Additional complexity arises from interfacial interactions between the blend components and both the substrate and free surface boundaries. If these interactions are not identical among the individual blend components, preferential segregation of at least one component to the corresponding interface may occur. Interfacial segregation in microphase separated diblock copolymer thin films[43] and immiscible binary homopolymer blend thin films[44] has been studied extensively. When the two blocks or homopolymers have dissimilar surface energies, the lower surface energy component will enrich the free surface. This phenomenon is exemplified by isotopic homopolymer mixtures, where the deuterated component enriches the free surface.[45,46] When the two blocks or homopolymers are chemically dissimilar, segregation to the film−substrate interface can be anticipated on the basis of the component having a more favorable enthalpic interaction with the substrate.[47−50] If the substrate is instead rendered chemically neutral to both components, preferential segregation can be avoided.[51] However, when there is no chemical dissimilarity between components, the preferred state of segregation of the film at a non-neutral substrate is more subtle. For polyolefin diblock copolymers, the conformationally more flexible block was shown to exclusively enrich the substrate−film interface for a variety of substrates.[52,53] Theoretical simulations of binary blends of conformationally asymmetric, but otherwise identical, homopolymers gave the same result.[54] In contrast, isotopic homopolymer mixtures have been shown to exhibit a transition in wetting behavior, with the lower and higher surface energy components enriching low and high surface energy substrates, respectively.[55,56] For pure block copolymers, the overall morphology of the film is dictated by a balance of these interfacial interactions and the inherent periodicity of the polymer. For binary homopolymer blends, both the thermodynamics and kinetics of macroscopic phase separation can be drastically altered by these interfacial phenomena. It is not obvious how the interplay between these various factors should affect the morphology in films containing symmetric combinations of homopolymers and their corresponding diblock copolymer. Furthermore, the phase behavior of symmetric ternary blends is extremely sensitive to composition in the vicinity of the BμE channel; therefore, nonuniform composition profiles imposed by preferential wetting conditions should be expected to have a significant impact on film morphology.

The only previously published comprehensive work regarding the phase behavior of thin films of symmetric ternary polymer blends, subject to the previously mentioned design constraints, was carried out by Stoykovich, et al.[57] and Liu, et al.[58] They investigated PS/poly(methyl methacrylate) (PMMA)/PS-PMMA

blends deposited on neutral substrates of silicon with a random copolymer of PS and PMMA grafted to the surface. The film thicknesses were matched to the equilibrium period of the PS-PMMA block copolymer. Under these conditions, the three characteristic morphologies occurring in the bulk as Φ_H is varied — lamellae, microemulsion, and macro-phase separation — are thermodynamically stable. In cases where the film thickness was 1.5 times the equilibrium period, preferential segregation of the homopolymers of the blend to the film—air interface was observed, although only for the microemulsion-forming blends. Furthermore, the microemulsions were not bicontinuous in nature, instead consisting of PS droplets in a continuous matrix of PMMA. Presumably, significant increases in film thickness, such that the film is no longer two-dimensional with respect to the microemulsion periodicity, may lead to morphologies more representative of a BμE.

From a practical standpoint, the neutralization of a substrate through a grafted polymer layer may be undesirable, for example, if direct contact is needed between the substrate and the film. This would be particularly important for the application of BμE templating strategies in functional devices requiring transport of matter or charge between adjacent layers. Therefore, we have studied the phase behavior of symmetric PE/PEP/PE—PEP blends on non-neutral substrates, including indium tin oxide (ITO), Si, and Ag. The blends were deposited at thicknesses greater than the bulk domain spacing of the BμE. After deposition, the films were annealed in the melt state to allow development of the equilibrium morphology. The annealing temperature and blend composition were selected to correspond to a BμE from previous investigations of the bulk properties of the blend. The film morphology was investigated by SEM observation after rendering the film porous by previously established techniques, namely crystallization of the PE and solvent extraction of the PEP. PE and PEP are simple hydrocarbons, hence there is no chemical basis to expect the preferential segregation of one component of the blend to either film interface. Nevertheless, we have found the steady state morphology of these films to result from macroscopic phase separation. We surmise that preferential segregation of blend components to the film interfaces is energetically driven, consequently altering the composition profile of the film and inducing an evolution of morphology from BμE to macro-phase separation. Fortunately, BμEs can be kinetically trapped with shorter annealing times to create film analogues of nanoporous PE monoliths. This work is an important first step toward the realization of new porous materials with structures templated by BμEs.

EXPERIMENTAL SECTION

PE, PEP, and PE—PEP with number-average molecular weights 23.0, 22.5, and 101 kg/mol, respectively, and narrow molecular weight distributions (polydispersity indices <1.1) were synthesized by anionic polymerization and catalytic hydrogenation of diene precursors following established procedures.[59] The PE—PEP diblock copolymer is symmetric, i.e., the volume fraction of PE is 0.50. The three polymers were dissolved in toluene at relative ratios corresponding to a ternary blend with volume fractions $\Phi_{PE} = \Phi_{PEP} = 0.425$ and $\Phi_{PE-PEP} = 0.15$. The amount of total polymer in solution was either 3 or 5% by weight. Films were prepared on various substrates by spin coating with a desktop precision instrument (Specialty Coating Systems, G3P-8), using a spin speed of 3000 rpm, acceleration times of 0.5—4 s, and a spinning duration of 60 s. Because PE and PE—PEP are intractable at room temperature, the spin coating was conducted at elevated temperature. The solution temperature varied from 72 to 100 °C, whereas the substrates and pipettes used to transfer the solution were held at 100 °C. In a typical run, a substrate was transferred from the hot plate to the spin coater chuck, and immediately thereafter, several drops of hot solution were deposited on the substrate and spinning was initiated. After coating, the films were further dried under vacuum to remove any residual toluene. The dried samples were then heated to 130 ± 2 °C in air for varying lengths of time to develop the melt morphology of the ternary blend film. Previous work has revealed that bulk ternary blends of PE, PEP, and PE—PEP, possessing identical chain lengths to the present system, exhibit a BμE morphology with $d \approx 160$ nm at the presently selected blend composition and annealing temperature.[20,21] Development of the film morphology was arrested by plunging the sample in liquid nitrogen; this induces crystallization of the PE domains in a manner which preserves the high temperature morphology of the blend.[60,61] Finally, the PEP homopolymer was selectively extracted from the solidified films by soaking in tetrahydrofuran (THF) for several minutes, followed by drying under vacuum.

Poly(tetrafluoroethylene) (PTFE), Si, indium tin oxide (ITO), and Ag were used as substrates. PTFE sheet was obtained from McMaster and cleaned successively in tergitol and deionized water, followed by ultrasonication twice in acetone and boiling in isopropanol for five minutes each. Polished n-type Si wafers (Cemat Silicon, crystal orientation (111)) were obtained from University Wafer and cleaned in acetone and isopropanol by an identical procedure. ITO was obtained from Colorado Concept Coatings, supplied as a ~150 nm coating on a thick glass substrate. The ITO substrates were cleaned by an identical procedure as that described for PTFE and were additionally exposed to UV/O_3 for 5 min using a Novascan PSD-UVT system. Polymer films were separately deposited on ITO substrates subjected only to solvent cleaning, as well as those subjected to both solvent and UV/O_3 cleaning. Ag substrates were prepared by thermal evaporation of a 75 nm layer on ITO substrates using an Angstrom Engineering EvoVac vacuum deposition system operated at 6×10^{-7} Torr.

The various substrates were selected to provide a range of surface energies with which to investigate film morphology. Therefore, surface energies were estimated through contact angle measurements. The contact angles of water and diiodomethane were measured on PTFE, Si, solvent-cleaned ITO, UV/O_3-treated ITO, and Ag using the sessile drop method via a Kruss G10 drop shape analysis system. Total surface energies were then calculated by the geometric mean approach, using the known surface energy components of water and diiodomethane.[62] The surface energy of the PTFE substrates calculated by this method was 12 mJ/m^2, in good agreement with the generally accepted value. The estimated surface energies of the solvent-cleaned ITO and Si substrates were 34 and 55 mJ/m^2, respectively. The UV/O_3-treated ITO substrates were completely wetted by diiodomethane, while the Ag substrates were completely wetted by both diiodomethane and water. Thus, although no values of the surface energy of these substrates could be estimated, we expect that their surface energies are greater than the Si substrates. More specifically, Ag should be expected to have the highest surface energy,[63] which is confirmed by the wetting behavior of both liquids.

Film thicknesses on Si substrates were evaluated immediately after spin coating and drying using a J. A. Woollam Co. variable angle spectroscopic ellipsometer. Spectra were collected from 700 to 950 nm with incident angles of 60 and 75°. The recorded data were fit using the Cauchy equation to extract film thickness. The average film thicknesses resulting from spin coating of 3 and 5% solutions were determined to be 224 and 508 nm, respectively. Significant difficulty was encountered in obtaining reasonable mean squared error in the curve fitting by this method. SEM analysis of the as-deposited films revealed periodic variations in thickness, i.e., large surface roughness, concomitant with these difficulties. Such considerations are further discussed in the Results section. Nevertheless, SEM observations of the film cross sections on Si

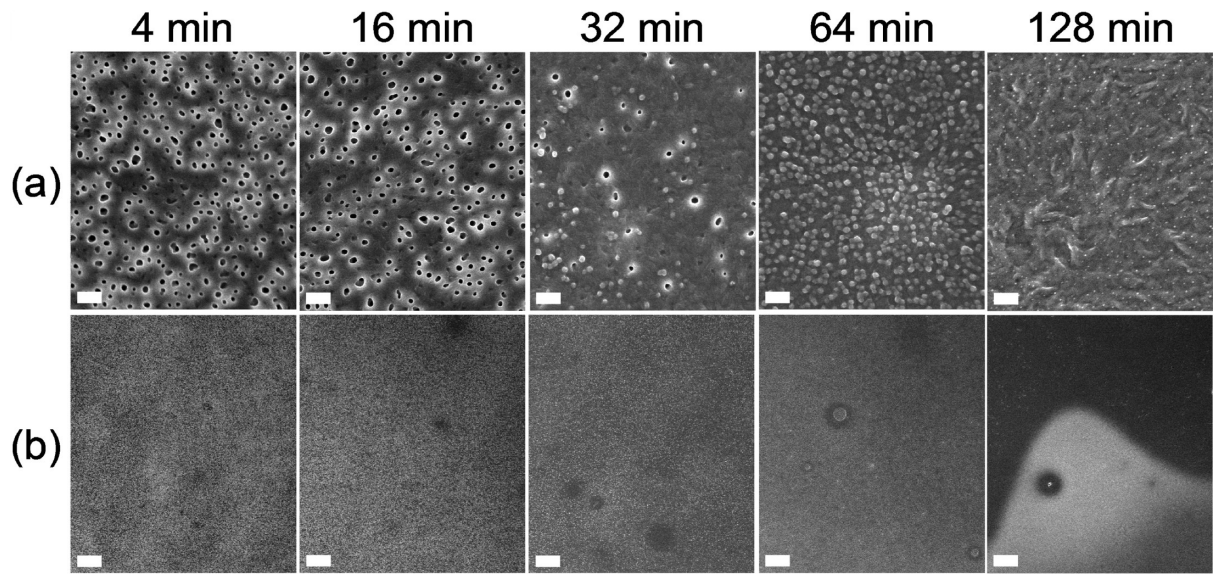

Figure 2. Plane-view (a) high- and (b) low-magnification SEM images of PE films on UV/O_3-treated ITO substrate after annealing at 130 °C for different times. Each image in (a) is a magnified view of the central region of the corresponding image in (b), except for 128 min, where the high-magnification view corresponds to the dark region of the low magnification view. The films were initially deposited by spin-coating from a 5 wt % solution at 3000 rpm and 72 °C. The scale bars indicate (a) 400 nm and (b) 10 μm.

confirmed, to a first approximation, the average thicknesses determined by ellipsometry. Moreover, the film cross sections on the other substrates indicated that similar thicknesses were obtained under identical spin-coating conditions.

SEM was conducted using a Hitachi S-900 instrument at operating voltages ranging from 2 to 5 keV. All samples were coated with ~20 Å of Pt metal prior to analysis, using a VCR indirect ion beam sputtering system. For the imaging of film cross sections, samples were fractured in liquid nitrogen, which was necessary in some cases to preserve the delicate pore structure of the films along the fracture plane.

RESULTS AND DISCUSSION

The surface energies of PE and PEP have previously been reported to be 28 and 24 mJ/m^2, respectively, at 130 °C.[56,64] On this basis, we expect the surface energies of the Si, ITO, and Ag substrates to be greater than all of the components comprising the ternary blends deposited on these substrates. In all cases investigated for this class of substrates, the ternary blend films exhibited a pronounced evolution of morphology, over a time scale of hours, when annealed in the melt state. This morphological evolution was monitored by trapping the melt morphology through crystallization of the PE and rendering the films porous by selective solvent extraction of the PEP homopolymer. The SEM images in Figure 2 show representative examples of the surface structure of such films after various annealing times; in these examples, the substrate is UV/O_3-treated ITO. Comparison of the surface structure at high and low magnification reveals an inverse correlation with time between the structural homogeneity at nanometer and micrometer length scales. After short annealing times, the high magnification views indicate a heterogeneous surface consisting of isolated pores with sizes roughly ranging from 50 to 150 nm. These pores should correspond to isolated domains of PEP prior to its selective extraction from the films. As time progresses, the density of pores at the surface decreases and, after 1−2 h, the surface is essentially featureless. Conversely, the low magnification views after short annealing times indicate that the isolated pores are distributed in a fairly uniform manner across the film; that is, no larger features are observed in the surface structure. This homogeneity at larger length scales persists through at least one hour of annealing. However, after 128 min, a drastic change is seen at low magnification, with the emergence of a heterogeneous structure consisting of large, randomly distributed, dark and bright regions. No further variation was observed after up to 1 day of annealing. The changes in surface structure at the two different length scales do not necessarily coincide. The progression toward homogeneity in part a of Figure 2 is apparent after only 32 min, whereas the appearance of heterogeneity in part b occurs between 64 and 128 min.

To gain further insight regarding the nature of the film morphologies on high surface energy substrates, we conducted thorough SEM analysis of the surface and cross-sectional structures existing after both short and long annealing times. Recalling that Φ_{PEP} = 0.425 in the ternary blends, the density of pores present at the film surface after short annealing times (Figure 2a) is less than expected, based purely on the overall composition of the film. Furthermore, the surface structure of Figure 2a is not reminiscent of a BμE, despite the fact that these blends unambiguously form BμEs in the bulk. However, examination of a typical surface at several different locations throughout the film revealed certain regions where the structure deviated from isolated pores. An example of such a region is provided in Figure 3a. In these instances, the surface structure is clearly more indicative of a BμE. In Figure 3b, the variation in surface structure from a BμE-like pore network to isolated pores over different regions of a film can be seen. It is important to note that the pore sizes in either case appear to range from roughly 50 to 150 nm, which is consistent with the pore sizes of nanoporous monoliths derived from the same blends.[20] The cross-sectional structure of the film after short annealing times, in contrast, is identical throughout the film and is shown in Figure 3c. The cross-section demonstrates that the interior of the film adopts a BμE morphology.

These observations can be collectively rationalized in the context of previous investigations regarding the phase behavior

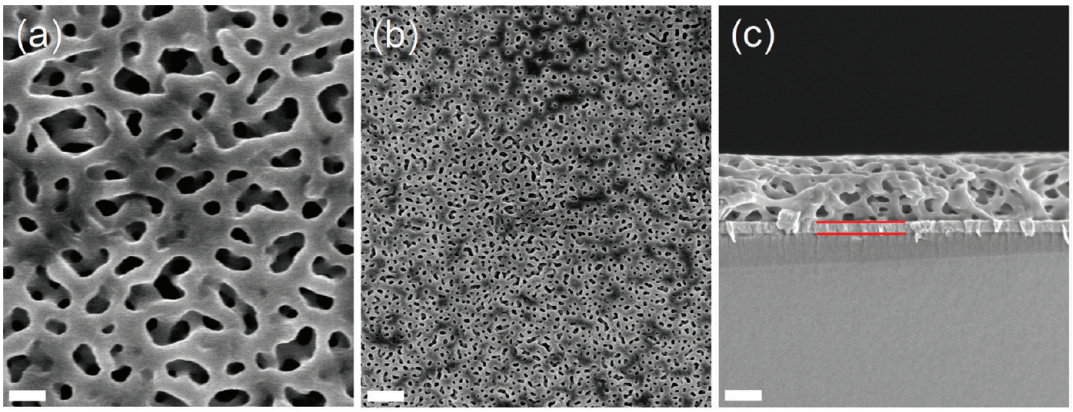

Figure 3. (a, b) Plane-view SEM images and (c) cross-section SEM image of PE film on UV/O_3-treated ITO substrate after annealing at 130 °C for 4 min. The image in (a) is a magnified view of the central region of the image in (b). The red lines in (c) demarcate the ITO, with the upper line indicating the ITO-film interface and the lower line indicating the ITO-glass interface. Scale bars indicate (a) 200 nm, (b) 1 μm, and (c) 400 nm.

of polymer blends near free surfaces. First, we assume that the PE, PEP, and PE−PEP are fairly homogeneously distributed throughout the film following the spin coating process (we acknowledge the possibility of macroscopic phase separation during spin coating;[65] however, based on the short time scales necessary to observe a BμE in these films, we feel that significant phase separation does not occur). When a film is first heated above the melting temperature of PE (~100 °C), the overall composition of the blend dictates that a BμE is the preferred morphology. The transition from a homogeneously mixed, single-phase state to a BμE is a disorder−disorder transition, and the diffusive length scales necessary for the blend to adopt a BμE are molecularly small. Thus, a BμE structure is observed (Figure 3c) after annealing times of only 4 min. Simultaneously, the blend components near the free surface are subject to disparate interactions with the surrounding medium, air. Previous studies have established that the lower surface energy component or, if the components are otherwise identical, the conformationally more flexible component will preferentially enrich the free surface in films of polymer blends or diblock copolymers.[45,46,52−54] PEP has a lower surface energy and statistical segment length than PE, and the PEP homopolymer in the present blends possesses the lowest molecular weight (surface energy roughly scales with the inverse of molecular weight[64]). Therefore, the PEP homopolymer should prefer to enrich the surface of these films over the PE homopolymer or PE−PEP diblock copolymer. We believe that the observed variation in surface structure results from local thickness variations in the film, as mentioned in the Experimental Section and discussed in more detail later. When the thickness coincides with an integral multiple of d, or perhaps an integral multiple of the natural period L_0 of the PE−PEP block copolymer, the thermodynamic factors driving the formation of a BμE overwhelm surface interactions and the free surface consequently exhibits a BμE structure. Otherwise, PEP is preferentially enriched at the free surface, resulting in a subsurface layer,[46,50,66−69] which is depleted in PEP and rich in PE and PE−PEP. The PEP-rich surface layer is removed when the film is soaked in THF, exposing the subsurface layer. Consequently, the surface in such regions exhibits a lower density of pores (PEP). This is consistent with previous work involving thin films of PS/PMMA/PS-PMMA ternary blends, where the film surfaces showed a microemulsion morphology and preferential segregation of homopolymer when the film thicknesses were comparable to integral and half-integral multiples of L_0, respectively.[58] Presumably, the decrease in the density of pores seen at the film surfaces upon increasing annealing time from 4 to 32 min results from further growth of the PEP-enriched surface layer and further depletion of PEP from the subsurface layer.

After long annealing times (≥128 min), SEM analysis of the films prepared on high surface energy substrates reveals that the heterogeneity in surface structure seen over large length scales (Figure 2b) arises from lateral, macroscopic phase separation. This phenomenon is summarized in Figure 4, again for the example of a UV/O_3-treated ITO substrate. To give a frame of reference, Figure 4(a) provides an additional view of the randomly distributed, bright and dark domains that result after 128 min of annealing. In the image, the sample is inclined at 45°, such that the surface and cross-section are simultaneously, partially visible. Examination of the surface within the bright domains (Figure 4b) reveals a distinctive granular structure characteristic of ITO. A pristine ITO surface, shown in Figure 4c, is provided for comparison, and a qualitatively similar surface structure is evident, although the granular structure is much more sharply defined. The poor structural definition of the bright domains in Figure 4b does not result from poor focusing in the microscope, but rather a low contrast level emanating from the sample. The SEM images are produced from the collection of secondary electrons, which are ejected from atoms existing at depths of, at most, several 10s of nm within the sample. The primary mechanism of contrast with secondary electrons is topology − secondary electron emission is strongly dependent on the angle of incidence of the sample surface with respect to the incident, primary electron beam. Thus, the low contrast level implies the presence of a surface layer which obscures the characteristic ITO structure. This is confirmed by a cross-section of the sample within a bright domain (Figure 4d), where a thin dense layer of thickness ~15 nm is clearly visible on the ITO. We believe this layer results from enrichment of the substrate−film interface by PE during annealing. This enrichment, coupled with that of the free surface by PEP, alters the overall blend composition in the interior of the film, such that macroscopically separated PE- and PEP-rich phases constitute the steady state morphology. The bright domains, then, correspond to PEP-rich regions that have been removed by THF, exposing a PE wetting layer. Conversely, the dark domains should correspond to PE-rich regions that are unaffected by THF. Indeed, the cross-section shown in Figure 4e

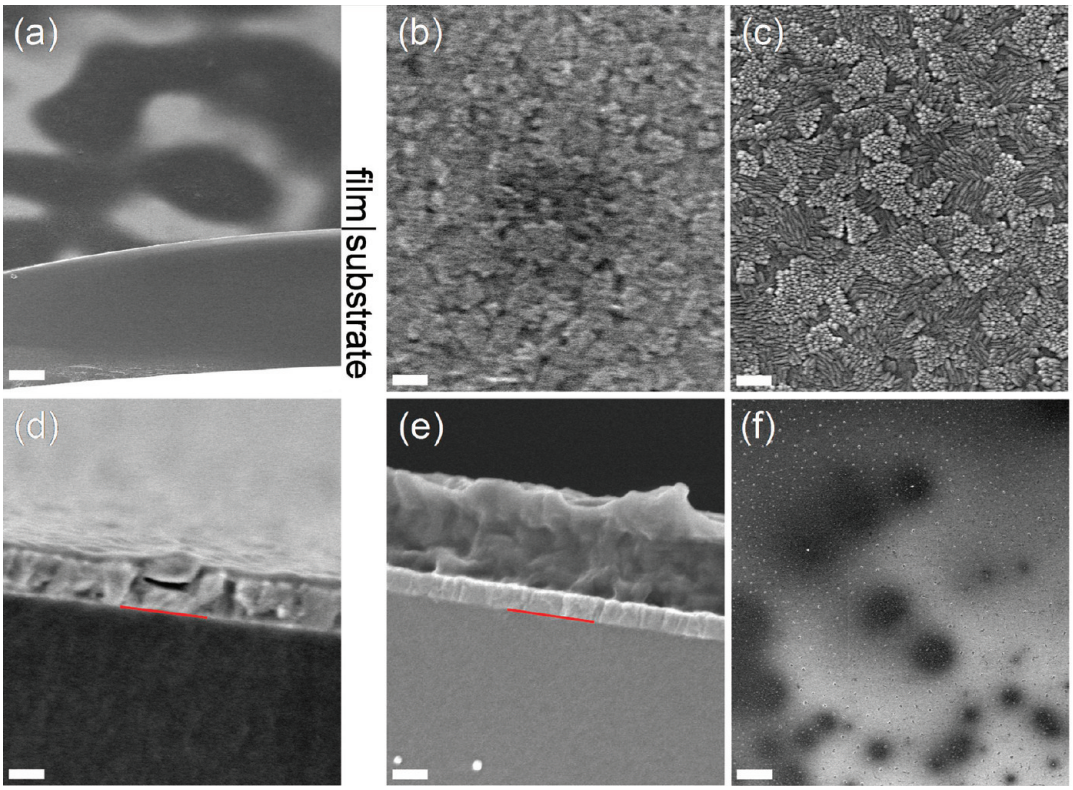

Figure 4. (a) SEM image of PE film on UV/O_3-treated ITO substrate after annealing at 130 °C for 128 min. The sample is inclined at 45° relative to the electron beam, such that the film and substrate are both visible as marked. (b) Plane-view, high magnification SEM image of typical surface structure corresponding to bright domains of (a). (c) Plane-view, high magnification SEM image of typical surface structure of ITO substrate prior to film deposition. (d, e) Cross-section SEM images corresponding to (d) bright and (e) dark domains of (a). The red lines indicate the ITO-glass interface in both cases. (f) Plane-view, SEM image of PE film on UV/O_3-treated ITO substrate after annealing at 130 °C for 22 h. Scale bars indicate (a) 10 μm, (b) 200 nm, (c) 200 nm, (d) 100 nm, (e) 200 nm, and (f) 10 μm.

demonstrates that these domains are essentially nonporous, with thicknesses comparable to the initial film thickness. The boundary between the dark and bright domains is not abrupt; analysis of cross-sections across boundaries reveals a progressive change in thickness from the limits shown in panels d and e in Figure 4, suggesting that phase separation perpendicular to the film plane may occur to some extent. Finally, further evidence of macroscopic phase separation is provided in Figure 4f. After long annealing times, certain regions of the films contained a large concentration of micrometer sized particles that appeared to be localized within the bright domains. Macroscopic phase separation in homopolymer blends containing a significant amount of diblock copolymer is known to proceed through the formation of complementary droplet microemulsions.[9] Thus, we infer that the particles residing within the bright domains are small PE particles that were encapsulated within a PEP matrix prior to its dissolution.

The transition with annealing time from a BμE to a macrophase separated morphology, and the apparent equilibrium nature of the latter, can be explained by considering a composition profile within a film. Figure 5 provides a general isothermal phase triangle for a ternary blend of type A/B/A−B. The overall, initial composition of the blends ($\Phi_H = 0.85$) is indicated by the red star; that is, the blends contain equal amounts of A and B and a small amount of A−B, such that a BμE is the equilibrium morphology. As the blends are annealed, we believe that PEP enrichs the free surface, as previously discussed. Furthermore,

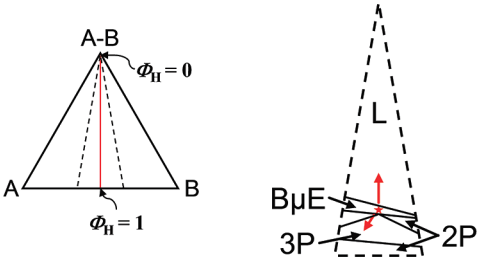

Figure 5. Idealized isothermal phase diagram for symmetric, bulk, A/B/A−B ternary polymer blends, showing the effect of depletion of individual components on the anticipated equilibrium morphology. On the left, the full ternary phase triangle is shown. The red line indicates the abscissa in the $T-\Phi_H$ phase diagram shown in Figure 1a and the end points $\Phi_H = 0$ and $\Phi_H = 1$ are marked. The dotted lines demarcate the region highlighted on the right, where theoretical boundaries are drawn between states consisting of microphase separated lamellae (L), BμE, and macroscopic phase separation into two (2P) or three (3P) phases (A-rich, B-rich, and BμE). A small region of coexistence separating the BμE and L phases is not shown. The boundary shapes will depend on the choice of A and B; however, the stability bias toward lower block copolymer content with increasing concentration of B is expected when B is the conformationally more flexible component.[15] The red star indicates the overall bulk composition of the blends in this work, while the red arrows indicate the resultant shift in composition from depletion of equal amounts of A−B and B or equal amounts of A and B.

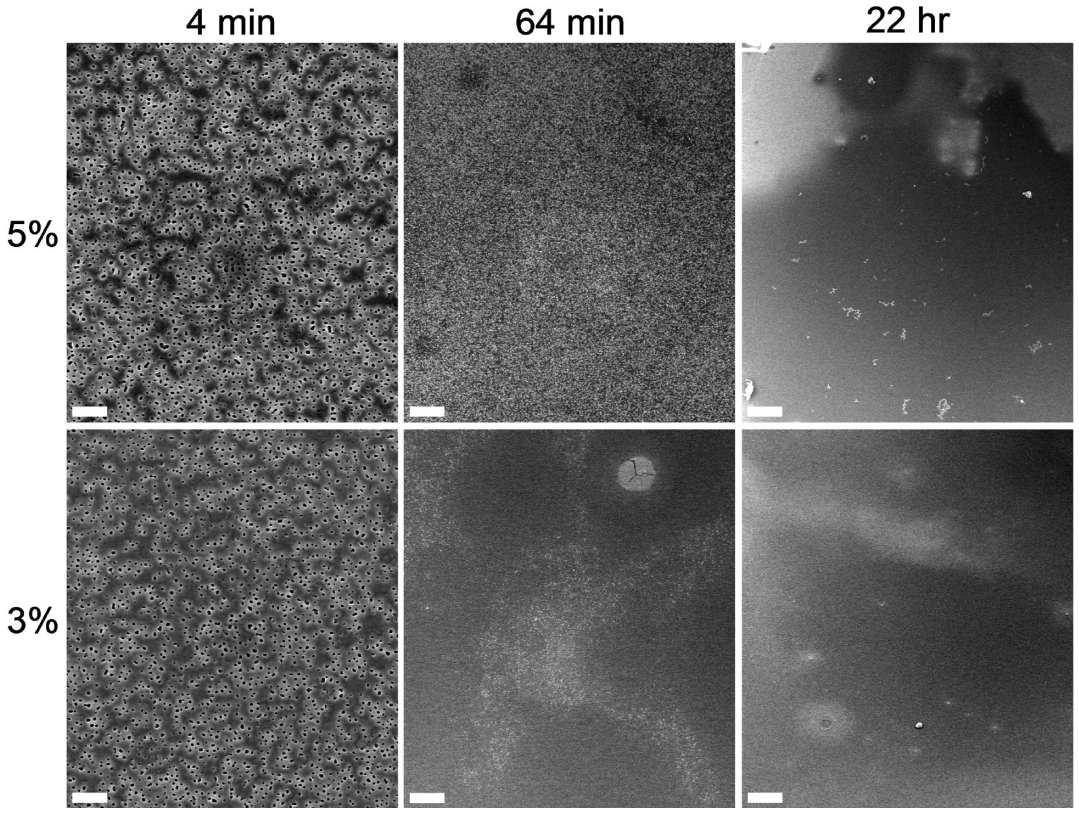

Figure 6. Plane-view SEM images of PE films with different thicknesses on Si substrate after annealing at 130 °C. The concentration of polymer in the spin coated solution is marked to the left and the annealing time is marked at the top of the images. The films were initially deposited at 3000 rpm and 72 °C. For 4 min, 64 min, and 22 h annealing, the images are high (scale bars, 1 μm), medium (scale bars, 10 μm), and low (scale bars, 40 μm) magnification, respectively.

Figure 4 demonstrates that PE enrichs the film−substrate interface, although from the figure alone we cannot discern whether the enriching species is the PE homopolymer, the PE block of the copolymer, or both. Now, consider the interior of the film as a ternary blend in equilibrium with PE (A) and PEP (B) wetting layers and depleted of those components. As the red arrows in Figure 5 show, if the PE wetting layer comprises entirely homopolymer, the blend composition shifts vertically toward an equilibrium of microphase separated lamellae. On the other hand, if the PE wetting layer comprises entirely the PE block of the copolymer, the blend composition shifts toward the lower left corner of the phase triangle, where the equilibrium state is macroscopic phase separation. Therefore, we propose that the nonequilibrium nature of a BμE on a high surface energy substrate is primarily due to segregation of the block copolymer to the film−substrate interface. Noting that the PE block of the copolymer is over twice the size of the PE homopolymer and, thus, should possess the higher surface energy, this hypothesis is consistent with previous work in which the higher surface energy component of isotopic homopolymer mixtures enriched the film−substrate interface for high surface energy substrates.[55,56] Moreover, the previously mapped bulk phase diagram for this system indicates that the BμE is stable over a range of ~2% in composition;[20,21] for a 500 nm thick film, the shift in composition, to a first approximation, by depletion of PE−PEP to a 15 nm thick wetting layer alone is 15/500, or 3%. Presumably, the BμE could be stabilized as the equilibrium morphology by adjusting the initial blend composition through the addition of excess PEP and PE−PEP, although we have not yet attempted such experiments.

Since the proposed mechanism underlying the evolution of morphology in these films relies on the formation of interfacial wetting layers, we consequently expect the kinetics of this transformation to depend on film thickness and substrate surface energy. Figure 6 summarizes the effect of variations in the former. In this example, the substrate is Si and comparatively thick and thin films have been deposited from 5 and 3 wt % polymer solutions, respectively. After short annealing times, the surfaces of both films exhibit the porous structure associated with a BμE in the interior of the film. After 64 min of annealing, the surface structure of the thicker film is relatively unchanged and there is no evidence of macroscopic phase separation. In contrast, the thinner film shows heterogeneous surface features associated with macroscopic phase separation. At steady state, both films adopt a macro-phase separated morphology, as evidenced after annealing for 22 h. Collectively, these results indicate that, while the initial and final morphologies of the films are identical, the transformation from BμE to macroscopic phase separation is triggered more quickly with decreasing thickness. This observation lends further support to the critical dependence of morphology on wetting phenomena for two reasons. First, the distance over which polymer chains must diffuse to support the formation of a wetting layer decreases with decreasing thickness. Second, the relative change in the blend composition resulting from depletion to a wetting layer should be magnified in thinner films, assuming the wetting layer thickness is not a strong

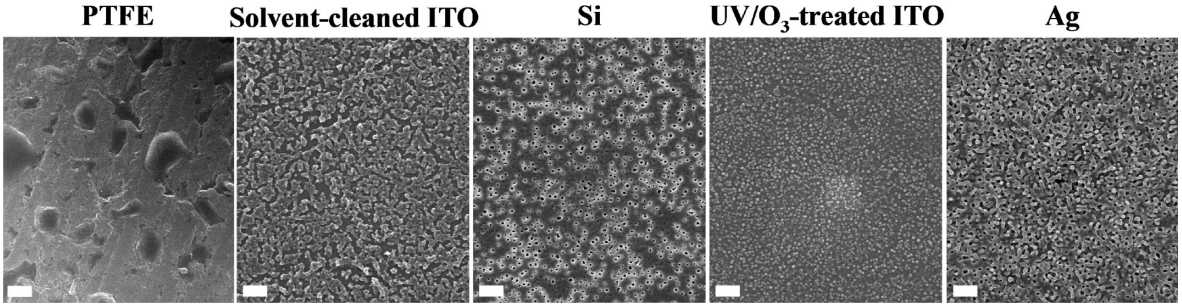

Figure 7. Plane-view SEM images of PE films prepared on substrates with surface energy increasing from left to right. The particular substrate used is indicated above the corresponding image. The films were initially deposited using a 5 wt % solution at 3000 rpm and 72 °C and then annealed at 130 °C for 64 min. The image for the film on PTFE is low magnification (scale bar, 40 μm), while the remaining images are high magnification (scale bar, 1 μm).

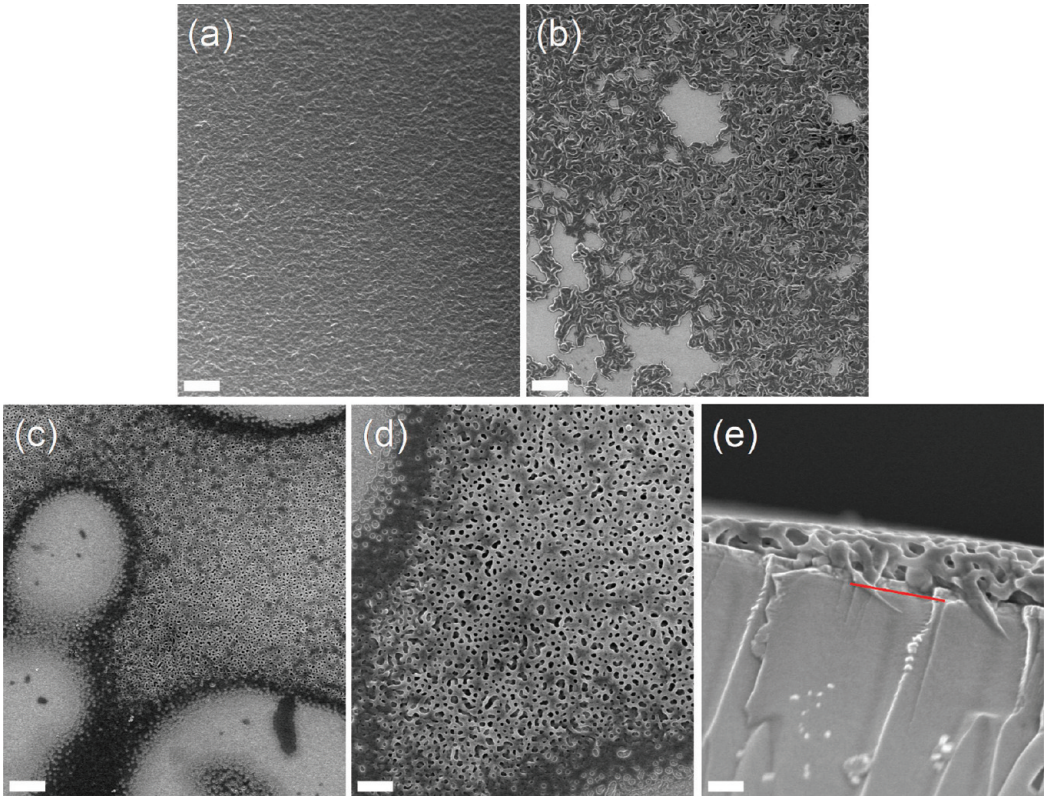

Figure 8. (a, b) Plane-view SEM images of as-deposited ternary blend (no annealing or PEP extraction) spin-coated on UV/O_3-treated ITO substrate from 5 wt % solution at 3000 rpm and (a) 72 °C and (b) 100 °C. Scale bars indicate 10 μm. (c, d) Top-down and (e) cross-section SEM images of nanoporous films having initial coverage similar to b, after annealing at 130 °C for 4 min. The cross-section corresponds to a lateral position in the film near the boundary between covered and exposed areas. The red line indicates the ITO-glass interface. Scale bars indicate (c) 2.5 μm, (d) 1 μm, and (e) 400 nm.

function of overall film thickness. The exact manner in which the shift of film morphology toward macroscopic phase separation is triggered likely involves interplay of these two factors.

In Figure 7, SEM images of films prepared on substrates of varying surface energy are shown. The films were prepared under otherwise identical conditions and annealed for 64 min. On the PTFE substrate, the film surface shows the formation of large islands of polymer, probably due to dewetting of the blend. The surface energy of both PE and PEP are significantly greater than the surface energy of PTFE, hence the blend is expected to display a finite contact angle on this surface. Films on the high surface energy substrates exclusively exhibited BμE and macro-phase separated morphologies over roughly comparable time scales, namely several minutes and several hours, respectively. However, as shown in Figure 7, the surface structures of these films were quite different after intermediate annealing times, suggesting a link between substrate surface energy or composition and the kinetics of the transformation. After 64 min annealing, the film surface on solvent-cleaned ITO appears to consist of networks of aggregated particles. On UV/O_3-treated ITO, the surface is populated by similarly sized and shaped, although unaggregated, particles. Meanwhile, the film surface on Si is essentially indistinguishable from those seen for all high surface energy substrates after short annealing times. Finally, the

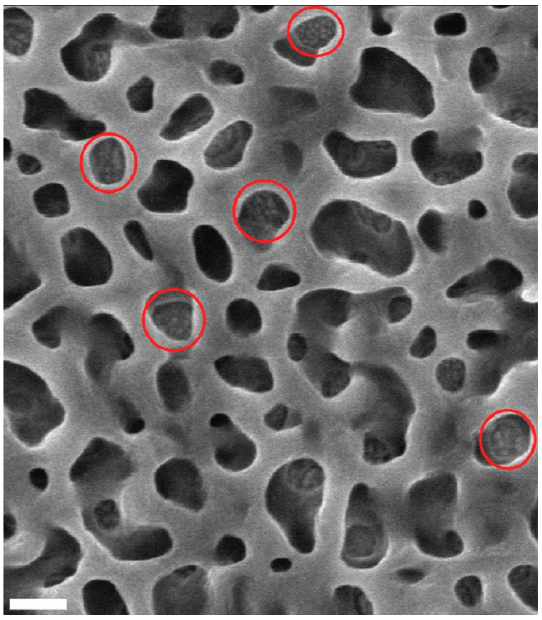

Figure 9. Plane-view SEM image of PE film demonstrating continuity of pore structure across both film interfaces. The film was prepared on a UV/O_3-treated ITO substrate using a 5 wt % solution and 4 min annealing time. The red circles highlight regions where the ITO substrate is visible through the pores. Scale bar indicates 200 nm.

film surface on Ag shows a morphology more or less representative of a BμE. We further note that, after 64 min annealing, low-magnification views of these film surfaces revealed the onset of macroscopic phase separation only for the solvent-cleaned ITO substrate. The surface structure of these films is clearly affected at intermediate stages by the choice of substrate in a complex manner. Undeniably, the kinetics of morphological evolution are dictated by the nature of the substrate and the exact manner in which wetting phenomena are induced. Additional experiments will be necessary to provide a clearer picture regarding the exact effect of substrate, for example by mapping the blend composition profile within the films.

Despite the fact that BμEs are nonequilibrium morphologies in these films, our results clearly show that BμEs can be kinetically trapped after only 4 min of annealing time. To reiterate, we are motivated to investigate the physics of these particular ternary blends on non-neutral substrates because of the availability of robust strategies by which BμE-derived, nanoporous PE can serve as a template in the synthesis of other nanoporous materials.[20,21] From a practical standpoint, the fact that BμE morphologies can be obtained in thin films by applying bulk principles and short annealing times is a valuable outcome. Another important aspect concerns the limiting, minimum film thickness at which a bicontinuous structure can be obtained. Rather fortuitously, we discovered that the various spin-coating parameters can be tuned, such that insight can be gained into the variation of morphology at very small film thicknesses using a single sample. Specifically, the level of substrate coverage by the ternary blend immediately after spin coating can be altered by controlling solution temperature. At lower temperatures, the substrate is completely covered and the film appears as shown in Figure 8a. As is evident, such films have high surface roughness; analysis of cross-sections indicates the variation in thickness after spin coating, but prior to annealing, to be on the order of 10s of nm. Films of this variety were exclusively used in the previously described experiments and the consequences of the roughness on the observed surface structure after annealing have been discussed. When the solution temperature is close to the boiling point of the solvent — toluene — the substrate is only partially covered, as shown in Figure 8b, with islands of polymer distributed among exposed areas of substrate. The local thickness of the film increases from zero at the boundaries between the islands and exposed areas to 100s of nm in the interior of the islands, i.e., over lateral distances corresponding to 10s of μm. With annealing, these films also show the same evolution of morphology from BμE to macroscopic phase separation. After short annealing times, the BμE structure exists in the interior of the islands, whereas after long annealing times, the films are indistinguishable from those having good initial coverage. In the former case, the morphology can be monitored as a function of thickness near the island boundaries; examples are shown in images c and d in Figure 8. As the film thickness increases in a region very close to these boundaries, the surface structure resembles droplets of PEP within a PE matrix, then dense PE, then a BμE. Within the islands, the surface structure alternates between BμE-like and isolated pores; as discussed before, we believe these latter two structures occur when the film thickness is matched or mismatched, respectively, with the periodicity of the blend. Remarkably, the cross-section of these films in the vicinity of the boundary regions reveals an essentially bicontinuous structure when the film thickness is roughly equal to d. Moreover, the areas where the film thickness is $\sim d$ correspond to the initial emergence of the BμE in the surface structure. Altogether, this suggests that a bicontinuous structure can be obtained in these systems, at minimum, for films with thicknesses comparable to the domain spacing of the BμE.

Lastly, we report one final observation regarding the structure of films possessing kinetically trapped BμEs. As shown in Figure 9, close inspection of the pore structure reveals that the substrate is visible through the pores in certain areas. This observation has significant practical implications regarding the applicability of these films as templates for the synthesis of other nanoporous films. Specifically, since the pores intersect the substrate, we expect that liquids infiltrated into the pores can directly contact the substrate. This should crucially enable the synthesis of templated films that are sufficiently adhered to the underlying substrate. Indeed, we have synthesized nanoporous conductive films, which will be described in a subsequent report.

CONCLUSIONS

We have detailed direct SEM investigations into the effect of confinement on BμE-forming ternary polyolefin blends. This represents the first comprehensive study of such systems on non-neutral substrates. The films were rendered nanoporous, not only as a means to observe their morphology, but also to demonstrate the viability of well-designed ternary polymer blends as precursors to films with bicontinuous porosity. We have discovered that bulk-equilibrium BμEs will macroscopically phase separate on high surface energy substrates because of preferential segregation of blend components to the film interfaces. This segregation is rationalized on an energetic basis and the phase separation was justified by considering its impact on the composition profile of the film. Considering the chemical similarity of PE and PEP, the results presented here are not expected to be generic for all symmetric, ternary blends; however, armed with sufficient knowledge of phase behavior in the bulk and the wetting preference of

blend components, one should be able to reasonably predict the equilibrium morphology in films of arbitrary blends. Critically, we also found that the films initially formed BμEs, which could be kinetically trapped by crystallization of PE. The BμE structure persists down to film thicknesses comparable to the periodicity of the microemulsion and the resultant nanoporous films possess pore networks continuous across both film interfaces. We anticipate that this work will lay the foundation for the extension of templating techniques to the synthesis of bicontinuous, nanoporous films of wide-ranging chemistry.

AUTHOR INFORMATION

Corresponding Author
*E-mail: lodge@umn.edu.

ACKNOWLEDGMENT

This work was supported by the MRSEC program of the National Science Foundation under Award DMR-0819885, the Abu Dhabi Minnesota Institute for Research Excellence (ADMIRE), a University of Minnesota Doctoral Dissertation Fellowship (BHJ), and the National Science Foundation Award ECCS-0925624 (KC). Portions of this work were carried out using instrumentation provided by the University of Minnesota Characterization Facility. We gratefully acknowledge Falah Al Hameli for performing contact angle measurements. We also acknowledge the assistance of Chris Frethem with SEM, Grant Lodden with ellipsometry, and Wieslaw Suszynski with contact angle measurements.

REFERENCES

(1) Scriven, L. E. *Nature* **1976**, *263*, 123–125.
(2) Ying, J. Y. *AIChE J.* **2000**, *46*, 1902–1906.
(3) Jackson, E. A.; Hillmyer, M. A. *ACS Nano* **2010**, *4*, 3548–3553.
(4) Haberkorn, N.; Lechmann, M. C.; Sohn, B. H.; Char, K.; Gutmann, J. S.; Theato, P. *Macromol. Rapid Commun.* **2009**, *30*, 1146–1166.
(5) Morris, R. E.; Wheatley, P. S. *Angew. Chem., Int. Ed.* **2008**, *47*, 4966–4981.
(6) Hamley, I. W. *Development in Block Copolymer Science and Technology*; Wiley: West Sussex, U.K., 2004.
(7) Hillmyer, M. A. *Adv. Polym. Sci.* **2005**, *190*, 137–181.
(8) Olson, D. A.; Chen, L.; Hillmyer, M. A. *Chem. Mater.* **2008**, *20*, 869–890.
(9) Bates, F. S.; Maurer, W. W.; Lipic, P. M.; Hillmyer, M. A.; Almdal, K.; Mortensen, K.; Fredrickson, G. H.; Lodge, T. P. *Phys. Rev. Lett.* **1997**, *79*, 849–852.
(10) Hillmyer, M. A.; Maurer, W. W.; Lodge, T. P.; Bates, F. S.; Almdal, K. *J. Phys. Chem. B* **1999**, *103*, 4814–4824.
(11) Washburn, N. R.; Lodge, T. P.; Bates, F. S. *J. Phys. Chem. B* **2000**, *104*, 6987–6997.
(12) Morkved, T. L.; Stepanek, P.; Krishnan, K.; Bates, F. S.; Lodge, T. P. *J. Chem. Phys.* **2001**, *114*, 7247–7259.
(13) Corvazier, L.; Messé, L.; Salou, C. L. O.; Young, R. N.; Fairclough, J. P. A.; Ryan, A. J. *J. Mater. Chem.* **2001**, *11*, 2864–2874.
(14) Pipich, V.; Schwahn, D.; Willner, L. *Appl. Phys. A: Mater. Sci. Process.* **2002**, *74*, S345–S347.
(15) Zhou, N.; Lodge, T. P.; Bates, F. S. *J. Phys. Chem. B* **2006**, *110*, 3979–3989.
(16) Broseta, D.; Fredrickson, G. H. *J. Chem. Phys.* **1990**, *93*, 2927–2938.
(17) Janert, P. K.; Schick, M. *Macromolecules* **1997**, *30*, 137–144.
(18) Kielhorn, L.; Muthukumar, M. *J. Chem. Phys.* **1997**, *107*, 5588–5608.
(19) Zhou, N.; Lodge, T. P.; Bates, F. S. *Nano Lett.* **2006**, *6*, 2354–2357.
(20) Jones, B. H.; Lodge, T. P. *Chem. Mater.* **2010**, *22*, 1279–1281.
(21) Jones, B. H.; Lodge, T. P. *J. Am. Chem. Soc.* **2009**, *131*, 1676–1677.
(22) Wang, H.; Oey, C. C.; Djurišić, A. B.; Xie, M. H.; Leung, Y. H.; Man, K. K. Y.; Chan, W. K.; Pandey, A.; Nunzi, J.-M.; Chui, P. C. *Appl. Phys. Lett.* **2005**, *87*, 023507.
(23) Crossland, E. J. W.; Kamperman, M.; Nedelcu, M.; Ducati, C.; Wiesner, U.; Smilgies, D.-M.; Toombes, G. E. S.; Hillmyer, M. A.; Ludwigs, S.; Steiner, U.; Snaith, H. J. *Nano Lett.* **2009**, *9*, 2807–2812.
(24) Perlich, J.; Kaune, G.; Memesa, M.; Gutmann, J. S.; Müller-Buschbaum, P. *Philos. Trans. R. Soc. Chem., Ser. A* **2009**, *367*, 1783–1798.
(25) Liu, Z.; Li, Y.; Zhao, Z.; Cui, Y.; Hara, K.; Miyauchi, M. *J. Mater. Chem.* **2010**, *20*, 492–497.
(26) Daoulas, K. C.; Müller, M.; Stoykovich, M. P.; Park, S.-M.; Papakonstantopoulos, Y. J.; de Pablo, J. J.; Nealey, P. F.; Solak, H. H. *Phys. Rev. Lett.* **2006**, *96*, 036104.
(27) Maex, K.; Baklanov, M. R.; Shamiryan, D.; Iacopi, F.; Brongersma, S. H.; Yanovitskaya, Z. S. *J. Appl. Phys.* **2003**, *93*, 8793–8841.
(28) Pai, R. A.; Humayun, R.; Schulberg, M. T.; Sengupta, A.; Sun, J.-N.; Watkins, J. J. *Science* **2004**, *303*, 507–510.
(29) Zhao, G.; Ishizaka, T.; Kasai, H.; Oikawa, H.; Nakanishi, H. *Chem. Mater.* **2007**, *19*, 1901–1905.
(30) Uehara, H.; Yoshida, T.; Kakiage, M.; Yamanobe, T.; Komoto, T.; Nomura, K.; Nakajima, K.; Matsuda, M. *Macromolecules* **2006**, *39*, 3971–3974.
(31) Phillip, W. A.; Amendt, M.; O'Neill, B.; Chen, L.; Hillmyer, M. A.; Cussler, E. L. *ACS Appl. Mater. Interfaces* **2009**, *1*, 472–480.
(32) Uehara, H.; Kakiage, M.; Sekiya, M.; Sakuma, D.; Yamonobe, T.; Takano, N.; Barraud, A.; Meurville, E.; Ryser, P. *ACS Nano* **2009**, *3*, 924–932.
(33) Walheim, S.; Schäffer, E.; Mlynek, J.; Steiner, U. *Science* **1999**, *283*, 520–522.
(34) Park, M. S.; Lee, Y.; Kim, J. K. *Chem. Mater.* **2005**, *17*, 3944–3950.
(35) Zhang, X.-T.; Sato, O.; Taguchi, M.; Einaga, Y.; Murakami, T.; Fujishima, A. *Chem. Mater.* **2005**, *17*, 696–700.
(36) Joo, W.; Park, M. S.; Kim, J. K. *Langmuir* **2006**, *22*, 7960–7963.
(37) Li, X.; Gao, J.; Xue, L.; Han, Y. *Adv. Funct. Mater.* **2010**, *20*, 259–265.
(38) Joo, W.; Kim, H. J.; Kim, J. K. *Langmuir* **2010**, *26*, 5110–5114.
(39) Li, X.; Xue, L.; Han, Y. *J. Mater. Chem.* **2011**, *21*, 5817–5826.
(40) Teubner, M.; Strey, R. *J. Chem. Phys.* **1987**, *87*, 3195–3200.
(41) Yin, Y.; Sun, P.; Jiang, R.; Li, B.; Chen, T.; Jin, Q.; Ding, D.; Shi, A.-C. *J. Chem. Phys.* **2006**, *124*, 184708.
(42) Ma, M.; Thomas, E. L.; Rutledge, G. C.; Yu, B.; Li, B.; Jin, Q.; Ding, D.; Shi, A.-C. *Macromolecules* **2010**, *43*, 3061–3071.
(43) Fasolka, M. J.; Mayes, A. M. *Annu. Rev. Mater. Res.* **2001**, *31*, 323–355.
(44) Geoghegan, M.; Krausch, G. *Prog. Polym. Sci.* **2003**, *28*, 261–302.
(45) Jones, R. A. L.; Norton, L. J.; Kramer, E. J.; Composto., R. J.; Stein, R. S.; Russell, T. P.; Mansour, A.; Karim, A.; Felcher, G. P.; Rafailovich, M. H.; Sokolov, J.; Zhao, X.; Schwarz, S. A. *Europhys. Lett.* **1990**, *12*, 41–46.
(46) Jones, R. A. L.; Norton, L. J.; Kramer, E. J.; Bates, F. S.; Wiltzius, P. *Phys. Rev. Lett.* **1991**, *66*, 1326–1329.
(47) Anastasiadis, S. H.; Russell, T. P.; Satija, S. K.; Majkrzak, C. F. *Phys. Rev. Lett.* **1989**, *62*, 1852–1855.
(48) Russell, T. P.; Coulon, G.; Deline, V. R.; Miller, D. C. *Macromolecules* **1989**, *22*, 4600–4606.
(49) Maaloum, M.; Ausserre, D.; Chatenay, D.; Coulon, G.; Gallot, Y. *Phys. Rev. Lett.* **1992**, *68*, 1575–1578.
(50) Bruder, F.; Brenn, R. *Phys. Rev. Lett.* **1992**, *69*, 624–627.
(51) Kellogg, G. J.; Walton, D. G.; Mayes, A. M.; Lambooy, P.; Russell, T. P.; Gallagher, P. D.; Satija, S. K. *Phys. Rev. Lett.* **1996**, *76*, 2503–2506.
(52) Sikka, M.; Singh, N.; Karim, A.; Bates, F. S.; Satija, S. K.; Majkrzak, C. F. *Phys. Rev. Lett.* **1993**, *70*, 307–310.
(53) Carignano, M. A.; Szleifer, I. *Europhys. Lett.* **1995**, *30*, 525–530.
(54) Wu, D. T.; Fredrickson, G. H.; Carton, J.-P. *J. Chem. Phys.* **1996**, *104*, 6387–6397.

(55) Krausch, G.; Dai, C.-A.; Kramer, E. J.; Marko, J. F.; Bates, F. S. *Macromolecules* **1993**, *26*, 5566–5571.
(56) Genzer, J.; Kramer, E. J. *Phys. Rev. Lett.* **1997**, *78*, 4946–4949.
(57) Stoykovich, M. P.; Edwards, E. W.; Solak, H. H.; Nealey, P. F. *Phys. Rev. Lett.* **2006**, *97*, 147802.
(58) Liu, G.; Stoykovich, M. P.; Ji, S.; Stuen, K. O.; Craig, G. S. W.; Nealey, P. F. *Macromolecules* **2009**, *42*, 3063–3072.
(59) Rosedale, J. H.; Bates, F. S.; Almdal, K.; Mortensen, K.; Wignall, G. D. *Macromolecules* **1995**, *28*, 1429–1443.
(60) Khandpur, A. K.; Macosko, C. W.; Bates, F. S. *J. Polym. Sci. Polym. Phys.* **1995**, *33*, 247–252.
(61) Loo, Y.-L.; Register, R. A.; Ryan, A. J. *Macromolecules* **2002**, *35*, 2365–2374.
(62) Owens, D. K.; Wendt, R. C. *J. Appl. Polym. Sci.* **1969**, *13*, 1741–1747.
(63) Israelachvilli, J. N. *Intramolecular & Surface Forces*, 3rd ed.; Academic: Burlington, VT, 2011.
(64) Sauer, B. B.; Dee, G. T. *Macromolecules* **1994**, *27*, 6112–6116.
(65) Heriot, S. Y.; Jones, R. A. L. *Nature* **2005**, *4*, 782–786.
(66) Krausch, G.; Dai, C.-A.; Kramer, E. J.; Bates, F. S. *Phys. Rev. Lett.* **1993**, *71*, 3669–3672.
(67) Steiner, U.; Klein, J.; Fetters, L. J. *Phys. Rev. Lett.* **1994**, *72*, 1498–1501.
(68) Krausch, G.; Kramer, E. J.; Bates, F. S.; Marko, J. F.; Brown, G.; Chakrabarti, A. *Macromolecules* **1994**, *27*, 6768–6776.
(69) Straub, W.; Bruder, F.; Brenn, R.; Krausch, G.; Bielefeldt, H.; Kirsch, A.; Marti, O.; Mlynek, J.; Marko, J. F. *Europhys. Lett.* **1995**, *29*, 353–358.